BRAIN COMMUNICATIONS

Loss of MINAR2 impairs motor function and causes Parkinson's disease-like symptoms in mice

⑩Rachel Xi-Yeen Ho,[1] Razie Amraei,[1] Kyle Oliver Corcino De La Cena,[1]
⑩Evan G. Sutherland,[1] Farzad Mortazavi,[2] ⑩Thor Stein,[1,3] Vipul Chitalia[4] and
⑩Nader Rahimi[1]

Parkinson's disease is the second most common human neurodegenerative disease. Motor control impairment represents a key clinical hallmark and primary clinical symptom of the disease, which is further characterized by the progressive loss of dopaminergic neurons in the substantia nigra pars compacta and the accumulation of α-synuclein aggregations. We have identified major intrinsically disordered NOTCH2-associated receptor 2 encoded by *KIAA1024L*, a previously uncharacterized protein that is highly conserved in humans and other species. In this study, we demonstrate that major intrinsically disordered NOTCH2-associated receptor 2 expression is significantly down-regulated in the frontal lobe brain of patients with Lewy body dementia. Major intrinsically disordered NOTCH2-associated receptor 2 is predominantly expressed in brain tissue and is particularly prominent in the midbrain. Major intrinsically disordered NOTCH2-associated receptor 2 interacts with neurogenic locus notch homologue protein 2 and is localized at the endoplasmic reticulum compartments. We generated major intrinsically disordered NOTCH2-associated receptor 2 knockout mouse and demonstrated that the loss of major intrinsically disordered NOTCH2-associated receptor 2 in mouse results in severe motor deficits such as rigidity and bradykinesia, gait abnormalities, reduced spontaneous locomotor and exploratory behaviour, symptoms that are highly similar to those observed in human Parkinson's spectrum disorders. Analysis of the major intrinsically disordered NOTCH2-associated receptor 2 knockout mice brain revealed significant anomalies in neuronal function and appearance including the loss of tyrosine hydroxylase-positive neurons in the pars compacta, which was accompanied by an up-regulation in α-synuclein protein expression. Taken together, these data demonstrate a previously unknown function for major intrinsically disordered NOTCH2-associated receptor 2 in the pathogenesis of Parkinson's spectrum disorders.

1　Department of Pathology, School of Medicine, Boston University Medical Campus, Boston, MA 02118, USA
2　Department of Anatomy and Neurobiology, School of Medicine, Boston University Medical Campus, Boston, MA 02118, USA
3　Boston University Alzheimer Disease and CTE Center, Boston University School of Medicine, Boston, MA, USA
4　Department of Medicine, Boston University School of Medicine, Boston, MA, USA

Correspondence to: Nader Rahimi, PhD Department of Pathology, Boston University Medical Campus
670 Albany Street, Room 510, Boston, MA 02118, USA
E-mail: nrahimi@bu.edu

Graphical Abstract

Introduction

Parkinson's disease is the second most common neurodegenerative disease and is characterized by motor symptoms such as resting tremor, bradykinesia, ataxia, rigidity and postural instability (Poewe *et al.*, 2017). Neuroanatomically, Parkinson's disease is characterized by progressive loss of dopaminergic neurons in the substantia nigra, accumulation and aggregates of α-synuclein protein in neuron bodies. Although significant progress has been made in understanding its neuropathology, Parkinson's disease still remains a progressive disorder that causes severe disability with no definitive causes or cures (Rizzo *et al.*, 2016; Poewe *et al.*, 2017).

Major intrinsically disordered NOTCH2-associated receptor 1 (MINAR1) was recently identified in our laboratory (Ho *et al.*, 2018). MINAR1 is a 916-amino-acid-long protein encoded by a previously uncharacterized gene, *KIAA1024*, which is located on chromosome 15q25.1. MINAR1 is composed of a long extracellular domain, a single transmembrane domain followed by a short cytoplasmic domain. Though it is considered to be a highly disordered protein, MINAR1 interaction with neurogenic locus notch homologue protein 2 (NOTCH2) increases its stability and function (Ho *et al.*, 2018). MINAR1 also interacts with and stabilizes DEP domain-containing mTOR-interacting protein, a negative regulator of the mammalian target of rapamycin complex 1 and mammalian target of rapamycin complex 2 signalling pathways (Zhang *et al.*, 2018). Initial characterization of MINAR1 revealed that MINAR1 inhibits angiogenesis and breast cancer growth in cell culture (Ho *et al.*, 2018). Consistent with its putative tumour suppressor function, MINAR1 expression is down-regulated in breast cancer (Ho *et al.*, 2018). In this study, we report the identification and characterization of major intrinsically disordered NOTCH2-associated receptor 2 (MINAR2) (previously known as uncharacterized protein KIAA1024L) as a second member of the MINAR family proteins. Similar to MINAR1, MINAR2 is predicated to have an extracellular domain, a single transmembrane domain with a few amino acids at the cytoplasmic domain. However, unlike MINAR1, MINAR2 encodes for a significantly smaller protein (i.e. 190 amino acid long) and is located on human chromosome 5q23.3 (mouse MINAR2 is located on Chromosome 18). MINAR2 is highly conserved in human and other species and is predominantly expressed in brain neuronal cells. To study the function of MINAR2, we have generated MINAR2 knockout (KO) mice and demonstrated that the loss of MINAR2 results in severe motor deficits, with symptoms that are highly congruent with those observed in human patients with Parkinson's disease. This underscores a critical and previously unknown function for MINAR2 in Parkinson's spectrum disorders.

Materials and Methods

Plasmids, antibodies and primers

MINAR2 (accession # NM_001257308.1) was amplified from a human brain cDNA library and was cloned into pMSCV-puro retroviral vector with the addition of Myc tag at C-terminus or into retroviral pLNCX^2 vector with a C-terminus green fluorescent protein (GFP). All the plasmids were sequenced before their use in cell culture. GFP-Lys-Asp-Glu-Leu plasmid was previously described (Maghsoudlou et al., 2016), and mEmerald-Calreticulin-N-16 plasmid (Cat #54023) was obtained from Addgene. A rabbit polyclonal anti-MINAR2 antibody was generated against human MINAR2 peptide (SLHTNLSGHLKENP), which is also conserved in mouse MINAR2 except the second residue (lysine, L, of human MINAR2 is replaced with valine, V, in mouse). The following primers were used for the genotyping of the MINAR2 KO mice:

CSD-LoxPcom-F1: GAGATGGCGCAACGCAATTAAT,
CSD-A730017C20Rik-R: TGAGTTCACTGCATACTTCT CCCTGG,
CSD-ttR: AATCCTTCCATTTACTGACTTCTCTCTC, and
CSD-F: CTCTATGACAGGGAAGCTAATGATTTG.

Animals

MINAR2 KO mice was generated by Wellcome Trust Sanger Institute [ESC clone ID: EPD0770_5_F06, Allele: A730017C20Riktm1b] (KOMP, Wtsi), which is on C57BL/6N background and obtained from the University of California, Davis, Mouse Biology Program. All mice used in this study were bred and maintained at Boston University Medical Campus after approval from the Institutional Animal Care and Use Committee. Five-month-old C57BL/6N wild type (WT) and MINAR2 KO mice were subjected to the behavioural assays listed below. Apart from the pole test, only female mice were employed in testing ($n = 5$ per group) as there were no significant differences in performance between male and female mice. Mice were introduced to the test room in advance for a 5-min acclimatization period and were allowed to rest for 10 min between trials. Test apparatus was thoroughly cleaned with 70% ethanol between each subject.

Cell culture studies

Human embryonic kidney (HEK)-293 cells expressing empty vector or MINAR2 were maintained in Dulbecco's Modified Eagle Medium supplemented with 10% foetal bovine serum and penicillin/streptomycin. Retroviruses were produced in 293-GPG cells (Rahimi et al., 2000). Viral supernatants were collected for 3 days, concentrated viruses were used to transduce into HEK-293 cells and infected cells were selected with puromycin or G418.

Western blotting and immunoprecipitation

Cells were prepared and lysed, and whole-cell lysates were subjected to Western blotting analysis using polyclonal anti-MINAR2 antibody or as indicated in the figure legends. In some occasions, whole-cell lysates were subjected to a co-immunoprecipitation assay, followed by Western blotting as indicated in the figure legends. Proteins were visualized using streptavidin–horseradish peroxidase-conjugated secondary antibody via chemiluminescence system. Cellulose acetate filter dot blot assay was carried out as described previously (Ho et al., 2018).

Pole test

The pole test is a simple method for evaluating motor dysfunction. WT ($n = 5$) and MINAR2 KO female ($n = 5$) and male ($n = 5$) mice were employed for this test. When positioned head-up on top of a 60-cm pole of 1-cm diameter, mice should be able to orient downwards and descend to the base. Recording starts when mice begin turning motions. Mice were given a maximum of 15 s to turn and allowed to remain on the pole for a maximum experiment run time of 30 s. Mice were assessed for the times taken to (i) turn their entire body downwards towards the base (turn time) and (ii) descend without sliding (descent time). If mice were unable to turn, they were assigned a turn time of 15 s. If they fell, slid or were not able to descend, they are removed and assigned the maximum descent time of 30 s. Each mouse was tested three times with a short period of rest between trials. The average turn time and descent time were taken for analysis.

Challenging balance beams

The challenging balance beams are a test of motor coordination. The set-up of the balance beams is as described previously (Carter et al., 1999). One-metre-long beams with a flat surface width of 15 and 7.5 mm are elevated between two wooden supports. A box with food or nesting material is placed at one end of the beam to encourage mice to cross the beam from the other end. Mice were trained to walk both beams three times at least 2 days before testing. Beginning with the 15-mm beam, mice are placed on the unsheltered end and allowed to traverse across the beam to the box on the other end. The latency to traverse and the number of paw slips are recorded. It is necessary to capture the walk on video to analyse the exact number of times the paw slips off the beam. The process is repeated with the 7.5-mm beam. The average traverse time and paw slips of two trials per group on each beam are noted for analysis (Carter et al., 1999).

Horizontal bars

The horizontal bar test is a common assessment of grip strength and motor coordination in mice. The apparatus consists of two interchangeable bars ∼38-cm long that are of 3 and 5 mm in diameter. The bars are held static between two wooden supports that are positioned ∼49 cm above the bench. Padding may be placed below the bars to break any falls. Beginning with the 3-mm bar, mice are held by the tail and positioned above the bars such that only their forepaws may grip the centre of the bar. Timing begins once the tail is released and the test is run for 30 s. Time is stopped if the subject falls before the maximum run time. A successful run involves either the subject remaining on the bar for 30 s or touching the support columns within the run time, for which the maximum score is awarded (see Deacon, 2013). This is repeated with the 5-mm bar. Performance of each subject is assigned a score as follows: 1–5 s = 1, 6–10 s = 2, 11–20 s = 3, 21–30 s = 4, after 30 s = 5, and one paw on the columns = 5. The total score for performance on both bars is tallied, and the average per group is taken.

Spontaneous activity in cylinder

The cylinder test evaluates sensorimotor ability by measuring spontaneous exploratory activity in the form of rearing and forelimb coordination in mice (Roome and Vanderluit, 2015). The transparent cylinder is set up such manner that the mouse may be videotaped from below. The mouse is placed in the cylinder and allowed to explore for 2 min. Noise was minimized to avoid startling subjects. The number of rears, defined as mouse standing on hind limbs and placing both fore paws on the walls of the cylinder, is recorded, and the average is taken.

Footprint assay

The paw print test is a straightforward method of observing motor dysfunction and movement disorders. The test evaluates motor coordination, balance and ataxia in mice by comparing patterns of gait. Mouse fore and hind paws are painted with non-toxic red and black paint, respectively. They were allowed to walk along a $60 \, cm \times 10 \, cm \times 10 \, cm$ walkway on top of a sheet of white paper. Gait was assessed through the measurements of: (i) stride length between the centres of successive hind paws, (ii) stride width between hind paw prints measured perpendicular to paw direction and (iii) foot overlap between the centres of succeeding fore and hind prints on one side. A total of five measurements were taken per parameter for each subject for analysis.

Immunofluorescence microscopy

Tissue sections were washed three times using 0.05 M Tris-buffered saline (TBS) (pH 7.6) for 5 min each to remove the cryoprotectant. The sections were blocked with SuperBlock Blocking Buffer (Thermo Scientific Product # 37515) [a Mouse on Mouse block (ABCAM) was used to block non-specific binding of antibodies that were made in mice]. Slices were incubated in the primary antibodies in a solution containing 2% normal goat serum (Gibco by Life Technologies), 0.1% Triton X (Fischer Scientific) in 0.05 M TBS, pH 7.6 (for 24 h at 4°C). Brain sections were then rinsed three times in 0.05 M TBS (pH 7.6) for 5 min each. Sections were then incubated with the appropriate secondary antibody conjugated to an fluorophore (goat anti-rabbit, or goat anti-mouse, Alexa 488 and Alexa 568, 1:1000) in a solution of 0.05 M TBS, pH 7.6, 0.1% Triton X for 2 h at room temperature while agitating on a rocker. This was followed by three 5-min washes with 0.05 M TBS (pH 7.6).

Transcardiac perfusion

Mice were intraperitoneally injected with a lethal dose of pentobarbital. A cannula was placed in the ascending aorta and 250 ml of 4% paraformaldehyde in 0.1 M phosphate buffer (pH 7.4) was perfused. The brain was immediately removed and fixed in 4% paraformaldehyde in 0.1 M phosphate buffer (pH 7.4) overnight, after which the brain was transferred to a series of glycerol solutions for 24 h each (10% glycerol, 2% dimethyl sulphoxide, followed by 20% glycerol, 2% dimethyl sulphoxide). Brains were then frozen at −80°C and sectioned into 40-μm-thick sections in the coronal plane using a freezing microtome. Serial sections were collected in a cryoprotectant solution and stored at −20°C. Human and non-human primate tissue: Paraformaldehyde-fixed brain tissue sections from age-matched non-Lewy body dementia (LBD) and patients with LBD or normal young adult Rhesus Monkey were used for the histological analysis and localization of MINAR2.

Statistical analysis

Two-sided unpaired *t*-test was used for compression among different datasets unless stated differently in the figure legends. The differences between datasets were considered significant at $P < 0.005$. The *P*-values are indicated on the figure or in the figure legends.

Data availability

Data and reagents are available from the corresponding author upon request.

Results

Identification of major intrinsically disordered NOTCH2-associated receptor 2 as a novel intrinsically disordered endoplasmic reticulum protein

After the original discovery of MINAR1 in our laboratory (Ho *et al.*, 2018), further analysis of the human genome identified the presence of another related gene with a significant homology with MINAR1, which was previously described as an unknown gene (KIAA1024L, accession # NM_001257308). Given the high degree of similarity to MINAR1, we recommended KIAA1024L be named MINAR2. As such, the accession # NM_001257308 in the National Center for Biotechnology Information dataset now corresponds to MINAR2 and, accordingly, the UniProt ID # of MINAR2 is P59773. MINAR2 amino acid sequence homology analysis revealed that MINAR2 is highly conserved in humans and other species such as mouse, rat, chimpanzee, bovine, cat and *Xenopus* (Supplementary Fig. 1), with human and mouse MINAR2 bearing a 79.38% similarity in amino acid sequences (Fig. 1A). MINAR2 is a 190-amino-acid protein that contains a predicated single transmembrane domain (Fig. 1A). This drastically differs from MINAR1, which is 916 amino acid long. In spite of the disparity in size, there is a high degree of homology between MINAR1 and MINAR2 amino acid sequences (Supplementary Fig. 2). Further analysis revealed that, similar to our previous characterization of MINAR1 as a largely disordered protein (Ho *et al.*, 2018), MINAR2 was also predicted to be an intrinsically disorder protein (Fig. 1B and C).

To investigate MINAR2 function, we cloned MINAR2 into retroviral pQCXIP vector with a C-terminus Myc tag or into retroviral pLNCX[2] vector with C-terminus GFP tag. Subsequently, MINAR2-Myc and MINAR2-GFP were retrovirally expressed in HEK-293 cells. Western blot analysis using anti-MINAR2 or c-Myc antibodies specifically detected MINAR2 with an apparent molecular weight of 26 kDa (Fig. 1D). The predicated molecular weight of MINAR2-Myc is 22 kDa, the apparent higher molecular weight of MINAR2 could be associated with its intrinsically disordered characteristic or due to post-translational modifications. The data also confirmed the specificity of anti-MINAR2 antibody, as no protein band was detected in control cells transduced with an empty vector (Fig. 1D).

Given that MINAR1 is characterized as and named for being an NOTCH2-binding protein with intrinsically disordered character (Ho *et al.*, 2018), we examined whether MINAR2 similarly binds to NOTCH2 and displays the characteristics of intrinsically disordered proteins. We demonstrated that MINAR2-Myc ectopically expressed in HEK-293 cells binds to endogenously expressed NOTCH2 in a co-immunoprecipitation assay (Supplementary Fig. 3A). To address whether MINAR2 is susceptible to protein aggregation, another feature of intrinsically disordered protein, we homogenized HEK-293 cells expressing empty vector or MINAR2-Myc and the resulting cell homogenate was applied to the cellulose acetate filter trap assay as described previously (Ho *et al.*, 2018). MINAR2 retained on the cellulose acetate filter (Supplementary Fig. 3B), indicating that MINAR2 is susceptible to protein aggregation, which is testament to the intrinsically disordered nature of MINAR2 protein.

We next sought to examine the cellular localization of MINAR2 in HEK-293 cells via immunofluorescence microscopy. Our initial immunofluorescence staining via anti-MINAR2 antibody (Fig. 1F) or c-Myc antibody (Fig. 1G) demonstrated that MINAR2-Myc was mostly present at the perinuclear compartments such as endoplasmic reticulum (ER) or Golgi apparatus. Staining of empty vector/HEK-293 cells with anti-MINAR2 antibody did not detect any staining (Fig. 1E), indicating that MINAR2 is not expressed at the detectable level in HEK-293 cells and that anti-MINAR2 antibody specifically detects MINAR2. Furthermore, live imaging of MINAR2-GFP/HEK-293 cells likewise showed that MINAR2 is localized at the perinuclear region of HEK-293 cells (Fig. 1H). To determine whether MINAR2 is localized at the ER compartments, we transfected MINAR2-Myc/HEK-293 cells with the ER markers Lys-Asp-Glu-Leu-GFP or calreticulin-GFP. The result showed that MINAR2 is prominently present at the ER compartments as it was co-localized with both Lys-Asp-Glu-Leu-GFP (Fig. 2A) and calreticulin-GFP (Fig. 2B) in HEK-293 cells. In addition, MINAR2 co-localized with Emerald-Golgi-7/beta-1,4-galactosyltransferase 1, another highly specific ER-marker (Supplementary Fig. 4). On the other hand, staining with mitochondria showed that MINAR2 is not localized at the mitochondria (Fig. 2C). Taken together, the data demonstrate that MINAR2 is an ER resident protein.

Major intrinsically disordered NOTCH2-associated receptor 2 is predominantly expressed in the brain

Our initial analysis of a panel of cell lines for the expression of MINAR2 showed that MINAR2 is not expressed in human kidney epithelial cells, monkey kidney cells (CV-1 in Origin, carrying the SV40 cells), mouse melanoma cells (B16F), kidney cancer cell lines (TK10 and 786-0) and colon cancer cell lines (DLD1 and human colorectal carcinoma cells) (Supplementary Fig. 5). Next, we decided to analyse the Expression Atlas (https://www.ebi.ac.uk/gxa/home), a publically available dataset, for
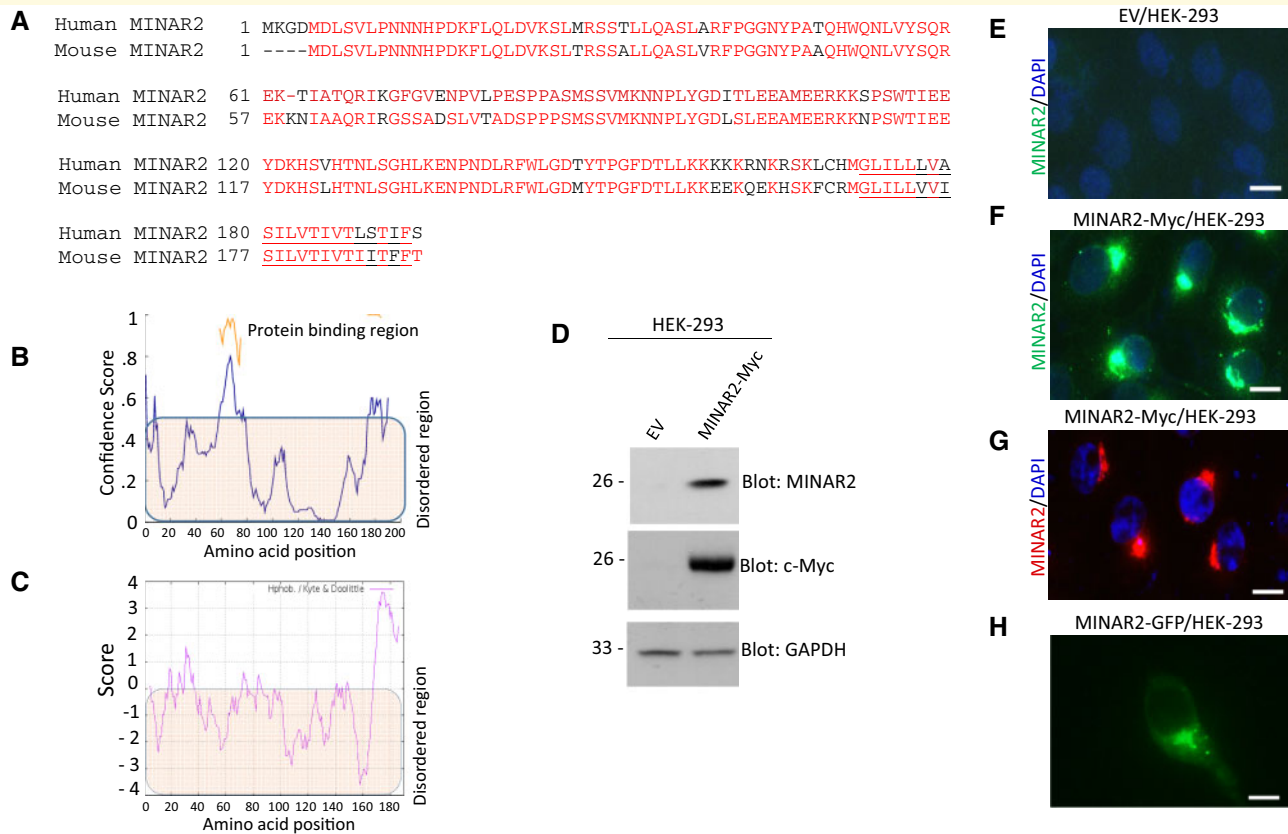
Figure 1 MINAR2 is a highly conserved intrinsically disordered protein. (**A**) Sequence homology of human MINAR2 (uniprot accession # P59773) and mouse (uniprot accession # Q8C4X7) is shown. (**B**) MINAR2 is predicated to be an intrinsically discorded protein. The graph was generated using online DISOPRED3 (Disorder Prediction) programme (http://web.expasy.org/protscale/). (**C**) The Kyte–Doolittle hydrophobicity score of MINAR2. (**D**) Western blot analysis of MINAR2-Myc from the cell lysates of HEK-293 cells expressing empty vector or MINAR2-Myc. Full uncropped Western blots are shown in Supplementary Fig. 11. (**E–G**) Immunofluorescence microscopy analysis of empty vector/HEK-293, MINAR2-Myc/HEK-293. (**H**) Live imaging of MINAR2-GFP/HEK-293 cells. Image magnification (20 µM).

MINAR2 expression. Our analysis revealed that MINAR2 is expressed in various regions of the human brain including the forebrain, midbrain, hindbrain and spinal cord (Supplementary Fig. 6). Further analysis of MINAR2 expression profile in mouse brain via the Protein Atlas (https://www.proteinatlas.org/) showed that MINAR2 is also expressed in equivalent regions of mouse brain, with the highest level of expression of MINAR2 located in the hypothalamus, midbrain and pituitary gland (Supplementary Fig. 7A). Moreover, analysis of *in situ* hybridization dataset on the mouse brain via Allen Institute for Brain Science/Allen Mouse Brain Atlas further illustrated that MINAR2 is expressed at high levels in various mouse brain regions (Supplementary Fig. 7B). Based on these observations, we decided to examine the expression of MINAR2 in non-human primate/rhesus monkey brain tissue via immunofluorescence staining. Our analysis reaffirmed dataset findings that MINAR2 is expressed in different regions of the brain including in the large pyramidal neurons in Layer 4 of primary motor cortex and those in the cerebellum (Fig. 3A and B). In

particular, the Purkinje cell layer of cerebellum was positive for MINAR2 as demonstrated by double staining of MINAR2 and parvalbumin (Fig. 3B). Additional analysis showed that expression of MINAR2 in non-human primate is not restricted to cells in the grey matter but is also expressed in the underlying white matter such as astrocytes (Fig. 3C) and microglia (Supplementary Fig. 8).

Generation of major intrinsically disordered NOTCH2-associated receptor 2 knockout mouse

To investigate the *in vivo* function of MINAR2, we obtained KO MINAR2 mice generated by inserting the L1L2_Bact_P cassette at Position 59071711 of Chromosome 18. The cassette is composed of a flippase recognition target site followed by a lacZ sequence and loxP site. The first loxP site was followed by neomycin under the control of the human β-actin promoter and SV40 polyA. MINAR2 was inserted at the third loxP site
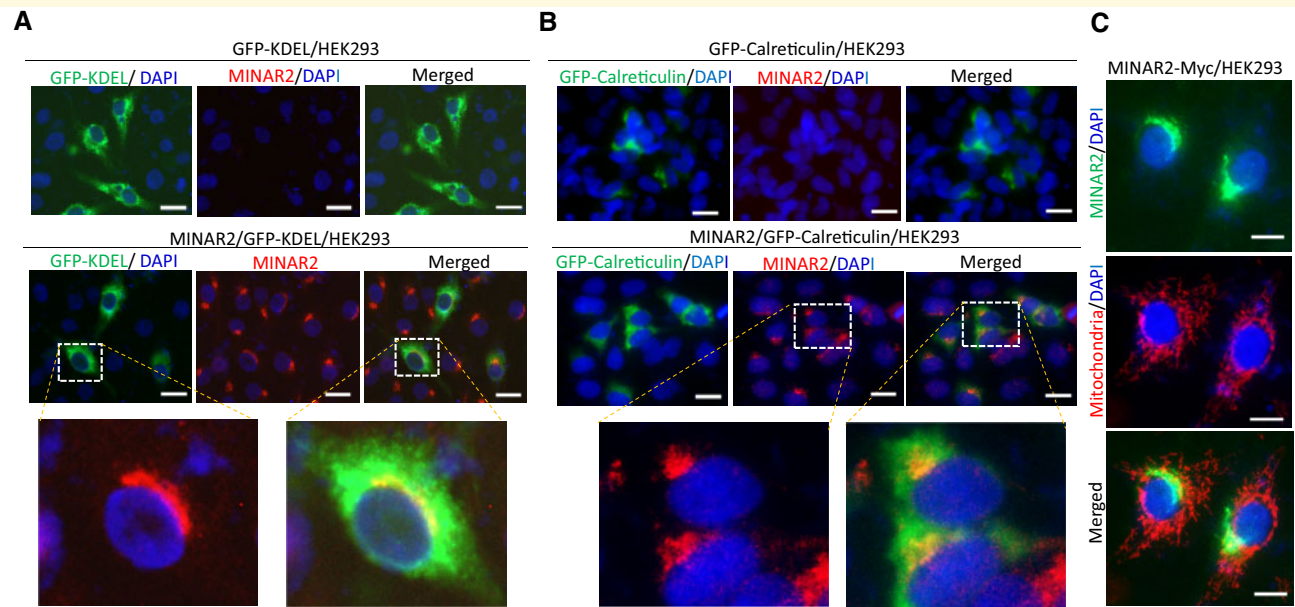
Figure 2 MINAR2 is localized at the ER. (**A**) HEK-293 and MINAR2/HEK-293 cells were transfected with a GFP-Lys-Asp-Glu-Leu construct. After 48 h of transfection, cells were fixed and stained with anti-MINAR2 antibody followed by immunofluorescence microscopy analysis. Image magnification (20 μM). (**B**) HEK-293 and MINAR2/HEK-293 cells were transfected with a GFP-Calreticulin construct after 48 h of transfection; cells were fixed and stained with anti-MINAR2 antibody followed by immunofluorescence microscopy analysis. Image magnification (50 μM). (**C**) MINAR2-Myc/HEK-293 cells were stained with mitochondria tracker. Image magnification (50 μM).

(Supplementary Fig. 9A). The total loss of MINAR2 in mice was confirmed by quantitative polymerase chain reaction (Supplementary Fig. 9B) and Western blotting (Supplementary Fig. 9C). Immunohistochemistry analysis showed that MINAR2 is widely expressed in the cortex and cerebellum of WT but not in MINAR2 KO mice (Supplementary Fig. 9D). In addition, MINAR2 staining of the cerebellum of WT mouse showed strong cytoplasmic positivity of MINAR2 in Purkinje cells (Supplementary Fig. 10), which are GABAergic neurons in cerebellum that are involved in motor coordination(Apps and Garwicz, 2005).

Loss of major intrinsically disordered NOTCH2-associated receptor 2 in mouse impairs motor function

During routine examination of MINAR2 KO mice, we noticed that these mice present with bradykinesia-like symptoms that were more prominent with older mice. Our initial tail suspension test revealed that MINAR2 KO mice display significantly delayed hind-limb reflex (Fig. 4A), indicating potential motor dysfunction such as bradykinesia and rigidity, which are classical hallmarks of neurodegenerative defects. The video further demonstrates that MINAR2 KO mice were unable to display hind-limb clasping behaviour seen in WT mice (Supplementary Videos 1 and 2). We used several well-

established motor function assessment tests to characterize the apparent motor deficits in MINAR2 KO mice. Specifically, we used the pole test, challenging balance beam and horizontal bar tests to evaluate different aspects of motor deficits in MINAR2 KO mice. In addition, we measured spontaneous locomotor activity via the cylinder test and ink-pad paw placement task to measure gait. For the pole test, which was originally developed to assess bradykinesia in mice with motor deficits (Matsuura et al., 1997), WT mice ($n = 5$, 6 months old) and MINAR2 KO female ($n = 5$, 6 months old) and male ($n = 5$, 6 months old) mice were assessed by measuring the time in seconds taken to fully orient downwards (turn time) and the total time taken to descend (descent time) the pole without sliding.

Considering that involuntary tremors are important diagnostic markers and indicators of movement disorders like Parkinson's disease, we examined if the motor abilities of MINAR2 KO mice were impaired. We used the pole test, challenging balance beam and horizontal bars to evaluate different aspects of motor coordination in MINAR2 KO mice. For the pole test, motor function for WT ($n = 5$) and MINAR2 KO female ($n = 5$) and male ($n = 5$) mice was assessed through measuring the time in seconds taken to fully orient downwards (turn time) and the total time taken to descend (descent time) the pole without sliding. The mean scores of turn time were 3.73 ± 1.81 s for WT, 14.3 ± 1.49 s for MINAR2 KO female and 13.1 ± 3.04 s for MINAR2 KO male mice
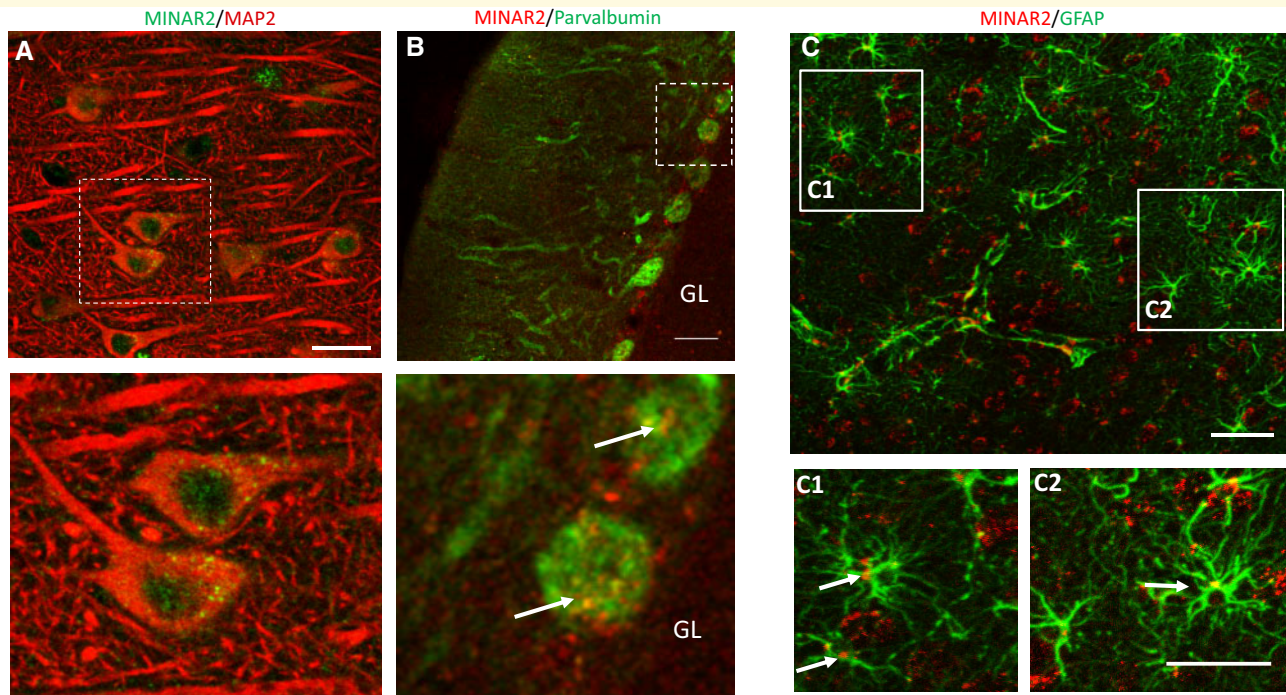
Figure 3 MINAR2 is expressed in non-human primate brain. (**A**) Rhesus monkey brain was co-stained with MINAR2 (green) and MAP2, microtubule-associated protein-2, a dendritic and neuronal marker (red) (scale bar = 20 μm). Higher magnification (lower panel corresponds to dotted box area) showing MINAR2 staining in the pyramidal neurons in Layer 4 of primary motor cortex. (**B**) MINAR2 (green) expression in Purkinje cells of the cerebellum of the rhesus monkey. Purkinje layer cells of the cerebellum are stained with parvalbumin (green) and MINAR2 (red) as well as cells in the GL (scale bar = 30 μm). Higher magnification (lower panel corresponds to dotted box area). (**C**) MINAR2 expression in astrocytes (red) of rhesus monkey white matter (GFAP, a marker for astrocytes, green). (**C1** and **C2**) Higher magnification showing the localization of MINAR2 to the cytoplasm of astrocytes. Expression of MINAR2 in nearby cells (oligodendroglia) also shown and in cells in the white matter as well as grey matter. Image magnification (50 μM). GL, granular layer.

(Fig. 4B, left panel). With regard to total descent time, WT mice took 12.1 ± 2.41 s, MINAR2 KO female took 28.3 ± 2.48 s and MINAR2 KO male took 26.4 ± 5.37 s (Fig. 4B, right panel). Comparing between WT mice and MINAR2 KO groups with Student's *t*-test, MINAR2 KO mice took significantly longer to turn ($P < 0.005$) and descend ($P < 0.005$) the pole than WT (Fig. 4B). The MINAR2 KO mice also exhibited difficulty in orienting downwards completely, sometimes with three limbs on one side of the pole, and they slid or fell down the pole instead of climbing down as WT mice did. The pole test demonstrated significant motor impairments in MINAR2 KO mice. The dramatic differences in the two measures from the pole test demonstrate that MINAR2 KO mice exhibit one of the cardinal symptoms of Parkinson's disease. Moreover, the symptoms observed in MINAR2 KO mice were independent of sex, as there were no appreciable differences observed in the motor impairments between MINAR2 KO male and female mice (Fig. 4B).

We further examined balance and fine motor coordination in MINAR2 KO mice by challenging them with balance beams of different widths. The amount of time taken to traverse the beams and the number of foot slips were measured and recorded. Although MINAR2 KO mice took slightly longer than WT mice to traverse the 7.5-mm beam, there were no significant differences in traverse time between both groups on the 15- and 7.5-mm beams (Fig. 5A, top left graph). However, there were significantly more foot slips made by MINAR2 KO mice (1.2 ± 1.14 slips) compared to WT mice (0.25 ± 0.463 slips) ($P < 0.05$). The difference in the number of foot slips was even greater when mice were challenged with the narrower 7.5-mm beam, with 3.3 ± 1.70 slips made by MINAR2 KO mice compared to just 1.33 ± 1.16 slips made by WT ($P < 0.005$) (Fig. 5A, top right graph). The significantly higher number of foot slips made by MINAR2 KO mice suggests that the mice experienced greater difficulty in maintaining balance and fine motor control.

To gain further insights into motor control impairment in MINAR2 KO mice, we measured forelimb grip strength of WT and MINAR2 KO mice using horizontal bar. The time spent on the bars and the ability to reach the wooden supports from the centre of the bars were scored. WT mice had no difficulties in gripping and traversing both 3- and 5-mm bars. In contrast, MINAR2 KO mice struggled to maintain grip and frequently failed to remain on the bar (Fig. 5B). MINAR2 KO mice
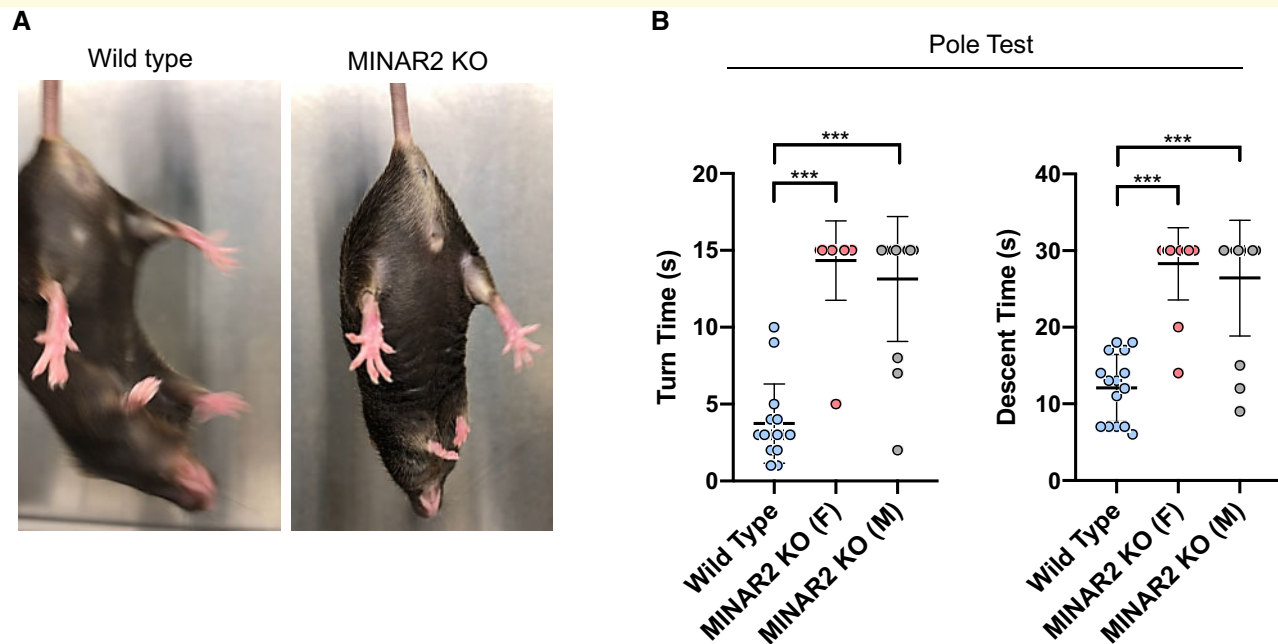
Figure 4 Loss of MINAR2 in mouse impairs motor function. (A) Posture of WT and MINAR2 KO mice in tail suspension test. **(B)** Six-month-old WT ($n = 5$) and MINAR2 KO ($n = 5$) were subjected to pole test and measured for turn time and descent time. Both MINAR2 KO female and male mice took a greater amount of time to turn and descend relative to WT mice. ***$P < 0.005$; Student's *t*-test. No differences were found between MINAR2 KO female and male mice performance.

performed significantly worse than WT, scoring 6.8 ± 0.837 for grip strength relative to a perfect score of 10 from WT ($P < 0.05$), indicating that MINAR2 KO mice had diminished grip strength relative to control (Fig. 5B).

Major intrinsically disordered NOTCH2-associated receptor 2 knockout mice display deficits in spontaneous locomotor and exploratory behaviour

We next measured spontaneous exploratory activity and forelimb coordination in MINAR2 KO mice in the cylinder test. The number of rears, defined as the mouse standing on hind limbs to rest both forepaws on the cylinder wall, for WT and MINAR2 KO mice was noted. WT mice reared a mean of 19 ± 3.74 times compared to a mean of 13.25 ± 3.77 rears in MINAR2 KO mice ($P < 0.005$) (Fig. 5C). WT mice began rearing activity nearly immediately in the new environment, and MINAR2 KO mice were slower to engage in exploratory behaviour (Fig. 5C). Interestingly, MINAR2 KO mice would attempt to rear by standing on their hind limbs but would often misjudge the distance by standing too far away from the wall or would only rest one forelimb on the wall. This apparent difference in rearing frequency

and ability suggests that loss of MINAR2 in mouse appears to impair sensorimotor function.

Major intrinsically disordered NOTCH2-associated receptor 2 knockout mice exhibit gait abnormalities that coincide with loss of dopaminergic neurons

Next, we subjected WT and MINAR2 KO mice to a footprint examination, which evaluates motor anomalies relating to gait pattern and is one of the few animal tests that are directly comparable to human gait analysis studies (Brooks *et al.*, 2012; Fleming *et al.*, 2013). Footprint patterns of mice walking down a narrow walkway were quantified by stride length, foot overlap and stride width. In general, MINAR2 KO mice appeared to meander from side to side through the walkway compared to WT mice (Fig. 6A). Statistical analysis showed that both WT and MINAR2 KO mice demonstrated overall comparable stride length (Fig. 6B). However, there were significant differences in footprint overlap between WT and MINAR2 KO mice (Fig. 6C). Footprint overlap is an indicator of step alteration; the shorter and less variation in the distance between fore and hind paws, the more uniform the step alteration as the mouse places its hind paws directly where the proceeding fore paw had been
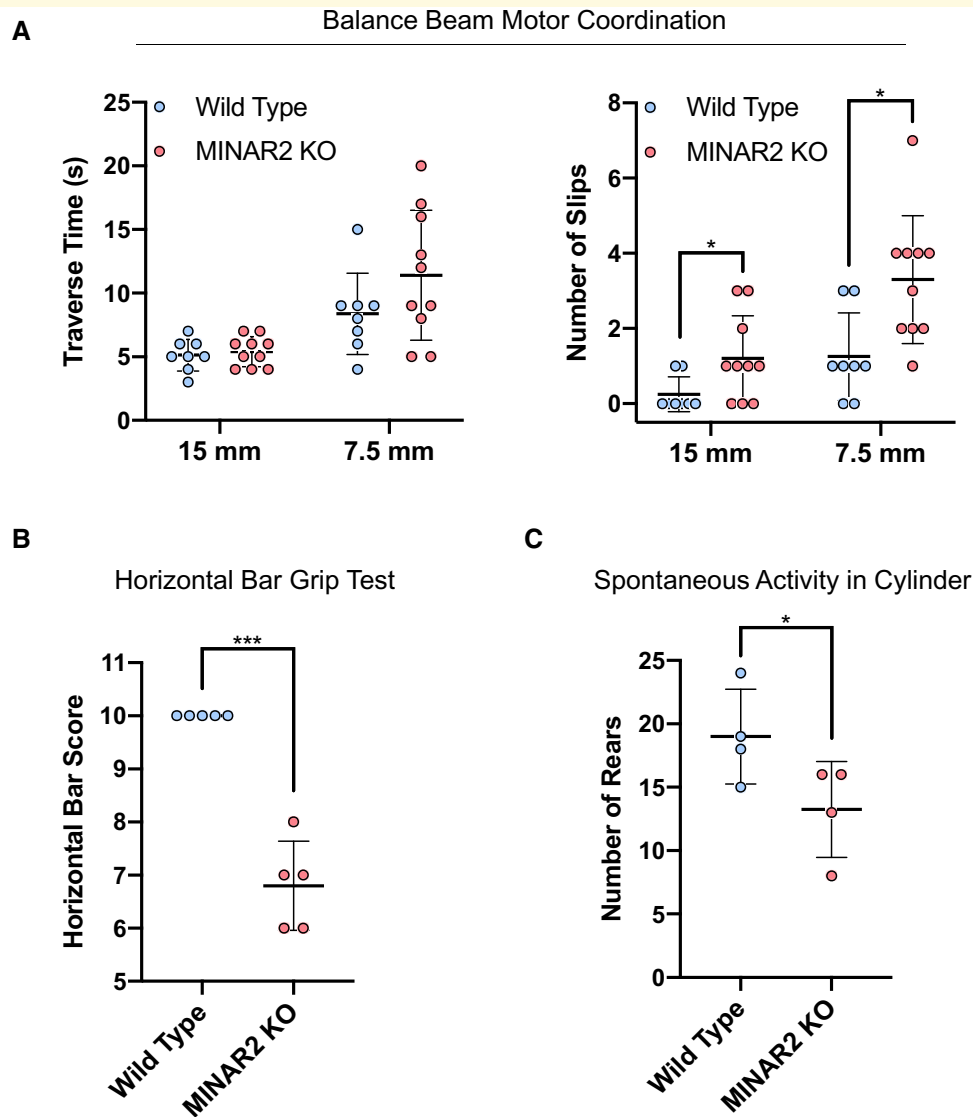
Figure 5 MINAR2 KO mice display locomotor function deficit. (**A**) Six-month-old WT ($n = 5$) and MINAR2 KO ($n = 5$) were subjected to balance beam test (traversing beams of 15 and 7.5 mm diameters), and mice were assessed for total traverse time (left graph) and the number of fore and hind foot slips (right graph). While no significant differences were detected in traverse time, MINAR2 KO mice exhibited more foot slips than WT on both 15-mm (*$P < 0.05$, Student's t-test) and 7.5-mm (***$P < 0.005$, Student's t-test) beams (right graph). (**B**) The same mice were evaluated for grip strength on horizontal bars. Mice were prompted to grip bars of 3 and 5 mm diameters. Latency to fall and success in touching the support columns was measured and scored. MINAR2 KO mice scored significantly lower for grip ability than WT mice. ***$P < 0.005$ (Student's t-test). (**C**) The same mice were subjected to spontaneous behaviour and locomotor ability assessment in clear cylinder. Mice were placed in a clear glass cylinder for 2 min and assessed for spontaneous activity through the number of rears against the glass wall. MINAR2 KO mice displayed significantly decreased incidences of rearing activity relative to WT. *$P < 0.05$ (Student's t-test).

(Fleming *et al.*, 2013). MINAR2 KO mice had a greater average distance of 1.02 ± 0.36 cm ($P < 0.05$) between ipsilateral fore and hind paw prints, nearly a third higher than WT mice that have an overlap distance of 0.68 ± 0.22 cm (Fig. 6C). Moreover, stride width between WT and MINAR2 KO mice was also markedly different (Fig. 6D). Overall, the results indicate that MINAR2 KO mice walk with more irregular, less uniform step alterations compared to WT mice. In addition, MINAR2 KO mice exhibited considerably more variability in stride

width length than WT ($P = 0.00253$), ranging from 2.2 to 3.5 cm compared to 2.5 to 3.3 cm, respectively (Fig. 6D). Together, the data indicate that MINAR2 KO mice possess distinct peculiarities in their gait pattern relative to WT mice.

Considering the observed bradykinesia and gait abnormalities in KO MINAR2 mice, we stained the brain of KO MINAR2 mice for tyrosine hydroxylase (TH). The aberrant expression of TH is associated with the degeneration of dopaminergic neurons in the substantia nigra,
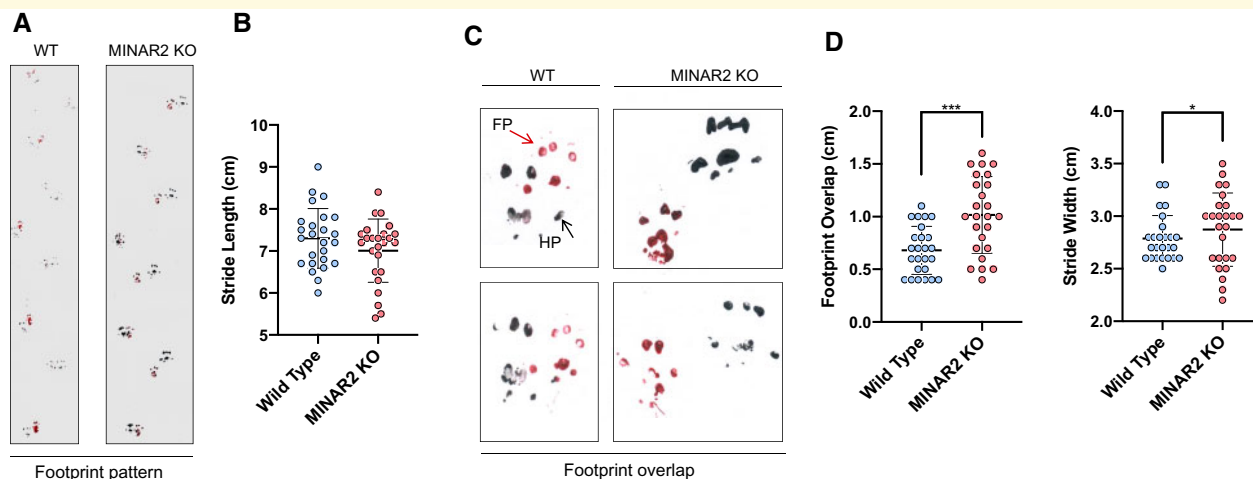
Figure 6 MINAR2 KO mice display gait abnormalities. (A) A representative footprint pattern of WT and MINAR2 KO is shown. **(B)** Stride length of WT and MINAR2 KO mice (6 months old, $n = 5$ per group). MINAR2 KO mice did not exhibit significant difference in the length between succeeding hind paw prints compared to WT. **(C)** A representative of footprint overlap of WT and MINAR2 mice is shown. FP and HP were painted red and black, respectively, as indicated by arrows. Graph is a representative of footprint of WT and MINAR2 KO mice (6 months old, $n = 5$ per group). The distance measured between succeeding fore and hind paw prints is increased in MINAR2 KO mice relative to WT, demonstrating less uniformity in step alteration. $P = 0.000169$. **(D)** Stride width of WT and MINAR2 KO is shown (6 months old, $n = 5$ per group). Measuring between opposing hind paw prints, MINAR2 KO mice showed significantly greater variation in gait width than control. $P = 0.00253$. FP, fore paw; HP, hind paw.

leading to a decrease in striatal dopamine levels. The TH staining of MINAR2 KO mice showed a far less densely packed tyrosine hydroxylase-immunoreactive neurons (i.e. pars compacta) as well as neurotic expression (i.e. reticulata) (Fig. 7A, WT compared to B, MINAR2 KO). Furthermore, double staining of the sections with TH (red) and α-synuclein (green) revealed as decrease in TH expression in MINAR2 KO mice (Fig. 7C, WT compared to D, MINAR2 KO), which was accompanied by an upregulation in the expression of α-synuclein protein (Fig. 7E, WT compared to F, MINAR2 KO).

Major intrinsically disordered NOTCH2-associated receptor 2 expression is down-regulated in the frontal lobe of patients with Lewy body dementia

Since loss of MINAR2 in mouse produced LBD-like phenotypes, in particular motor dysfunction, we decided to examine MINAR2 expression in the brains of three age-matched patients clinically diagnosed with LBD. Our analysis revealed that MINAR2 expression is significantly reduced in the frontal lobe brain of patients with LBD compared to age-matched non-LBD individuals (Fig. 8A–D). The reduced expression of MINAR2 in the frontal-lobe of patients with LBD appeared to be selective as levels of MINAR2 expression in the cerebellum of patients with LBD were similar to that of non-LBD patients (Fig. 8A–D). The staining of midbrain with MINAR2 did

not produce any useful information as the midbrain of patients with LBD was largely devoid of neurons (data not shown). Needless to say that, given the small number of patients, no robust conclusions can be made at this time. However, the data suggest that reduced MINAR2 expression in patients with LBD could play a role in the pathology of LBD.

Discussion

Motor dysfunction is the salient incapacitating feature of a considerable number of human neurological and neuromuscular diseases, including Parkinson's disease (Brundin et al., 2015; Nalls et al., 2015). Patients with Parkinson's disease often suffer from sensorimotor impairments, including bradykinesia, tremors and rigidity, conditions that only worsen over time. In this study, we demonstrate that MINAR2 is predominantly expressed in the brain, particularly in midbrain. The loss of MINAR2 in mouse results in several indices of motor dysfunction. Consistent with known pathologies of motor function impairment, the MINAR2 KO mice brain has significant alterations in neuronal function including loss of TH positive neurons in the pars compacta, which was accompanied by the accumulation of α-synuclein protein.

Various behavioural tests including tail suspension, pole test and challenging balance beam tests demonstrated a substantial motor impairment with MINAR2 KO mice. Likewise, the footprint assay, which is commonly used method for assessing gait in mouse (Brooks et al., 2012),
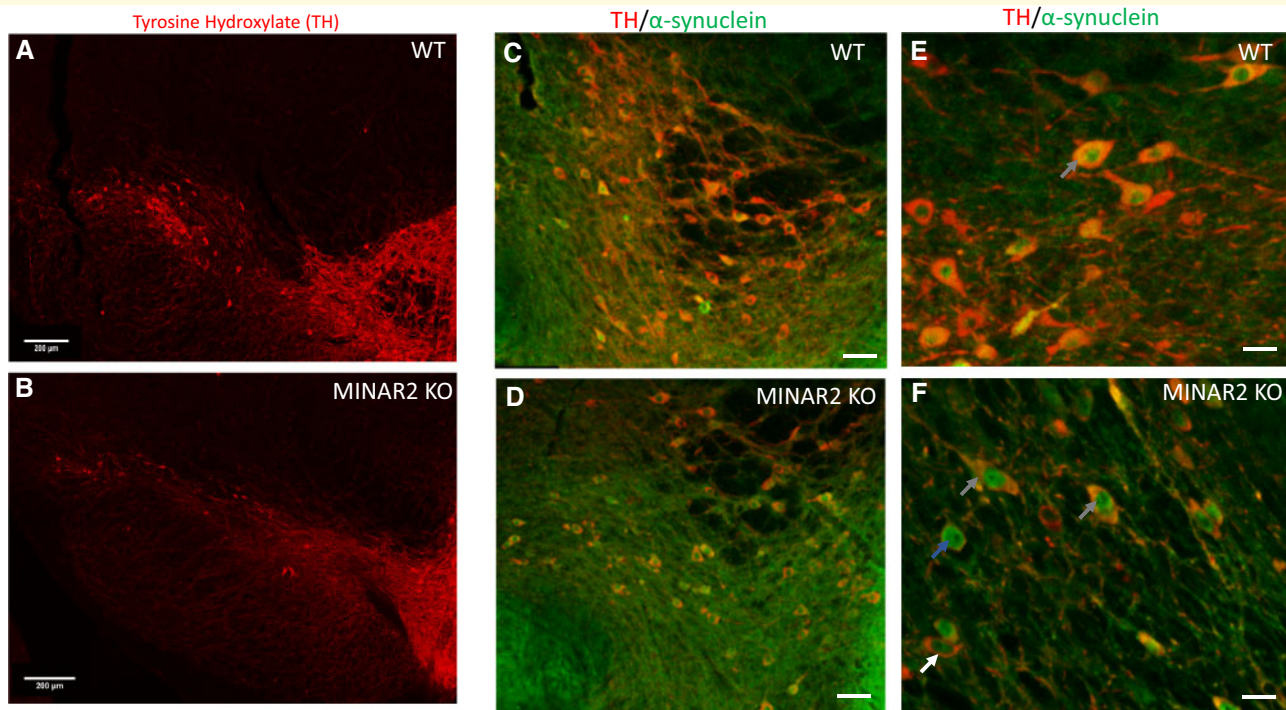
Figure 7 Loss of MINAR2 impairs TH positive cells in substantia nigra pars compacta. (**A** and **B**) Confocal images of tyrosine hydroxylase (TH) staining in Substantia Nigra pars compacta in WT and MINAR2 KO mice. There are significantly less number of TH+ neurons in KO compared to WT. Decreased neuritic expression of TH in the Substantia Nigra pars reticulata is also observed in MINAR2 KO mice. Image magnification (200 μM). (**C** and **D**) Confocal images of TH (red) and α-synuclein (green) staining in Substantia Nigra pars compacta of WT and MINAR2 KO mice. There are a significantly less number of TH+ neurons in MINAR2 KO compared to WT and accompanied by an up-regulation of α-synuclein. Grey arrow point to TH+ cell, while still expressing TH; green arrow shows TH− neurons that are mostly α-synuclein positive. (**E** and **F**) There are also neurons that express both TH and α-synuclein. WT mice show normal expression levels of TH and endogenous α-synuclein. Neuritic α-synuclein is also up-regulated, and very few TH+ neurites are observed compared to WT mice (E compared to F) (scale bars = 10 μm).

also showed motor dysfunction and movement abnormality in MINAR2 KO mice. Furthermore, when MINAR2 KO mice were evaluated via horizontal bar test, a common assessment for grip strength and motor coordination in mice (Deacon, 2013), the mice demonstrated major impairments in the motor function. In addition, the spontaneous activity in cylinder and challenging beam tests, which are widely used methods to measure sensorimotor function in mouse models of Parkinson's disease (Goldberg et al., 2003; Fleming et al., 2013), revealed that MINAR2 KO mice developed impairment in the sensorimotor function.

The most common characteristic features of Parkinson's disease are neuronal loss in specific areas of the substantia nigra pars compacta and widespread intracellular α-synuclein accumulation (Dickson et al., 2009; Halliday et al., 2011). Our analysis of the brain of MINAR2 KO mice revealed that TH-positive neurons in the compacta were significantly reduced in both density and TH expression. More importantly, this was accompanied by an up-regulation in the expression of α-synuclein, suggesting that loss of MINAR2 in mice is associated with Parkinson's disease-like symptoms. Interestingly, the pathological hallmark of Parkinson's disease is the formation of neuronal cytoplasmic inclusions of insoluble proteins called Lewy bodies, which is composed of mostly aggregates of misfolded α-synuclein. Our analysis of the brain (frontal lobe) of age-matched patients with LBD (three patients) demonstrated that MINAR2 is selectively down-regulated compared to non-LBD patients, suggesting a potential role for MINAR2 in the pathogenesis of LBD. Curiously, MINAR2 is localized to ER compartments and interacts with NOTCH2. ER stress, NOTCH folding, and its trafficking from the ER have been proposed to play a role in the progression of Parkinson's disease (Okajima et al., 2005; Mercado et al., 2016; Coppola-Segovia et al., 2017; Lee et al., 2019). Under physiological conditions, α-synuclein is degraded by autophagy and the ubiquitin/proteasome. Under pathological conditions, the failure in these systems contributes to its toxicity and accumulation in cells leading to ER stress(Chu et al., 2009; Winslow et al., 2010; Decressac and Bjorklund, 2013). However, extensive work is required to probe the precise function of MINAR2 in the ER.
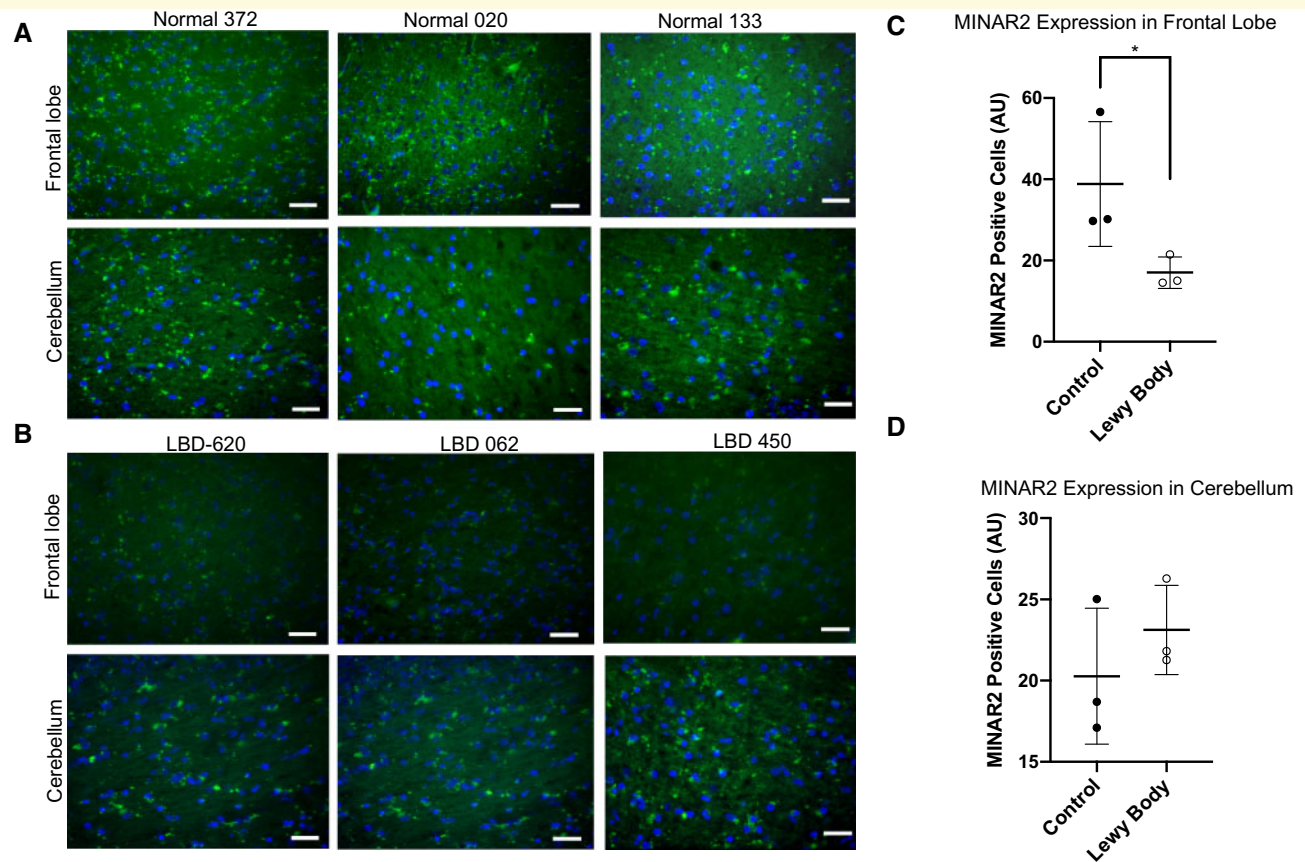
Figure 8 MINAR2 expression is selectively down-regulated in the frontal lobe brain of patients with LBD. Brain sections (frontal lobe and cerebellum) of three age-matched normal/non-LBD (# 372, 026 and 133) and three patients with LBD (# 620, 062 and 450) were stained with MINAR2. (**A**) Staining of the frontal lobe and cerebellum of the age-matched normal brain for MINAR2 (MINAR2, green and DAPI, blue). Image magnification (50 μM). (**B**) Staining of the frontal lobe and cerebellum of the LBD patients brain for MINAR2 (MINAR2, green and DAPI, blue). Image magnification (50 μM). (**C** and **D**) Quantification of MINAR2-positive neurons in frontal lobe and cerebellum of the control and patients with LBD.

Despite intense research on the pathogenesis of Parkinson's disease, the mechanisms that trigger neuronal loss and disease progression remain unknown. Not surprisingly, there are currently no specific tests for Parkinson's disease, with diagnosis typically relying on the assessment of patients' medical history of physical and neurological symptoms. The data presented in this manuscript identifies MINAR2, a previously uncharacterized protein, as potentially significant player in Parkinson's disease pathology. Further studies including those aiming to examine the expression profile of MINAR2 in patients with Parkinson's disease and mechanistic studies in cell culture and mice are required to fully appreciate the potential role of MINAR2 in diseases associated with the motor dysfunction.

Supplementary material

Supplementary material is available at *Brain Communications* online.

Funding

Competing interests

The authors report no competing interests.

References

Apps R, Garwicz M. Anatomical and physiological foundations of cerebellar information processing. Nat Rev Neurosci 2005; 6: 297–311.

Brooks SP, Trueman RC, Dunnett SB. Assessment of motor coordination and balance in mice using the rotarod, elevated bridge, and footprint tests. Curr Protoc Mouse Biol 2012; 2: 37–53.

Brundin P, Atkin G, Lamberts JT. Basic science breaks through: New therapeutic advances in Parkinson's disease. Mov Disord 2015; 30: 1521–7.

Carter RJ, Lione LA, Humby T, Mangiarini L, Mahal A, Bates GP, et al. Characterization of progressive motor deficits in mice transgenic for the human Huntington's disease mutation. J Neurosci 1999; 19: 3248–57.

Chu Y, Dodiya H, Aebischer P, Olanow CW, Kordower JH. Alterations in lysosomal and proteasomal markers in Parkinson's disease: relationship to alpha-synuclein inclusions. Neurobiol Dis 2009; 35: 385–98.

Coppola-Segovia V, Cavarsan C, Maia FG, Ferraz AC, Nakao LS, Lima MM, et al. ER stress induced by tunicamycin triggers alpha-synuclein oligomerization, dopaminergic neurons death and locomotor impairment: a new model of Parkinson's disease. Mol Neurobiol 2017; 54: 5798–806.

Deacon R. Measuring motor coordination in mice. J Vis Exp 2013; 79: e2609.

Decressac M, Bjorklund A. TFEB: pathogenic role and therapeutic target in Parkinson disease. Autophagy 2013; 9: 1244–6.

Dickson DW, Braak H, Duda JE, Duyckaerts C, Gasser T, Halliday GM, et al. Neuropathological assessment of Parkinson's disease: refining the diagnostic criteria. Lancet Neurol 2009; 8: 1150–7.

Fleming SM, Ekhator OR, Ghisays V. Assessment of sensorimotor function in mouse models of Parkinson's disease. J Vis Exp 2013; 76: 50303.

Goldberg MS, Fleming SM, Palacino JJ, Cepeda C, Lam HA, Bhatnagar A, et al. Parkin-deficient mice exhibit nigrostriatal deficits but not loss of dopaminergic neurons. J Biol Chem 2003; 278: 43628–35.

Halliday GM, Holton JL, Revesz T, Dickson DW. Neuropathology underlying clinical variability in patients with synucleinopathies. Acta Neuropathol 2011; 122: 187–204.

Ho RX-Y, Meyer RD, Chandler KB, Ersoy E, Park M, Bondzie PA, et al. MINAR1 is a Notch2-binding protein that inhibits angiogenesis and breast cancer growth. J Mol Cell Biol 2018; 10: 195–204.

Lee JH, Han J-H, Kim H, Park SM, Joe E-H, Jou I. Parkinson's disease-associated LRRK2-G2019S mutant acts through regulation of SERCA activity to control ER stress in astrocytes. Acta Neuropathol Commun 2019; 7: 68.

Maghsoudlou A, Meyer RD, Rezazadeh K, Arafa E, Pudney J, Hartsough E, et al. RNF121 inhibits angiogenic growth factor signaling by restricting cell surface expression of VEGFR-2. Traffic 2016; 17: 289–300.

Matsuura K, Kabuto H, Makino H, Ogawa N. Pole test is a useful method for evaluating the mouse movement disorder caused by striatal dopamine depletion. J Neurosci Methods 1997; 73: 45–8.

Mercado G, Castillo V, Soto P, Sidhu A. ER stress and Parkinson's disease: pathological inputs that converge into the secretory pathway. Brain Res 2016; 1648: 626–32.

Nalls MA, McLean CY, Rick J, Eberly S, Hutten SJ, Gwinn K, et al. Diagnosis of Parkinson's disease on the basis of clinical and genetic classification: a population-based modelling study. Lancet Neurol 2015; 14: 1002–9.

Okajima T, Xu A, Lei L, Irvine KD. Chaperone activity of protein O-fucosyltransferase 1 promotes notch receptor folding. Science 2005; 307: 1599–603.

Poewe W, Seppi K, Tanner CM, Halliday GM, Brundin P, Volkmann J, et al. Parkinson disease. Nat Rev Dis Primers 2017; 3: 17013.

Rahimi N, Dayanir V, Lashkari K. Receptor chimeras indicate that the vascular endothelial growth factor receptor-1 (VEGFR-1) modulates mitogenic activity of VEGFR-2 in endothelial cells. J Biol Chem 2000; 275: 16986–92.

Rizzo G, Copetti M, Arcuti S, Martino D, Fontana A, Logroscino G. Accuracy of clinical diagnosis of Parkinson disease: A systematic review and meta-analysis. Neurology 2016; 86: 566–76.

Roome RB, Vanderluit JL. Paw-dragging: a novel, sensitive analysis of the mouse cylinder test. J Vis Exp 2015; 79: e52701.

Winslow AR, Chen CW, Corrochano S, Acevedo-Arozena A, Gordon DE, Peden AA, et al. alpha-Synuclein impairs macroautophagy: implications for Parkinson's disease. J Cell Biol 2010; 190: 1023–37.

Zhang H, Zhang Q, Gao G, Wang X, Wang T, Kong Z, et al. UBTOR/KIAA1024 regulates neurite outgrowth and neoplasia through mTOR signaling. PLoS Genet 2018; 14: e1007583.